

SCIENTIFIC REPORTS



OPEN

Deep sub-wavelength nanofocusing of UV-visible light by hyperbolic metamaterials

Minkyung Kim¹, Sunae So¹, Kan Yao², Yongmin Liu^{2,3} & Junsuk Rho^{1,4}

Received: 29 June 2016
Accepted: 11 November 2016
Published: 07 December 2016

Confining light into a sub-wavelength area has been challenging due to the natural phenomenon of diffraction. In this paper, we report deep sub-wavelength focusing via dispersion engineering based on hyperbolic metamaterials. Hyperbolic metamaterials, which can be realized by alternating layers of metal and dielectric, are materials showing opposite signs of effective permittivity along the radial and the tangential direction. They can be designed to exhibit a nearly-flat open isofrequency curve originated from the large-negative permittivity in the radial direction and small-positive one in the tangential direction. Thanks to the ultraflat dispersion relation and curved geometry of the multilayer stack, hyperlenses can magnify or demagnify an incident beam without diffraction depending on the incident direction. We numerically show that hyperlens-based nanofocusing device can compress a Gaussian beam down to tens-of-nanometers of spot size in the ultraviolet (UV) and visible frequency range. We also report four types of hyperlenses using different material combinations to span the entire range of visible frequencies. The nanofocusing device based on the hyperlenses, unlike conventional lithography, works under ordinary light source without complex optics system, giving rise to practical applications including truly nanoscale lithography and deep sub-wavelength scale confinement.

Recently, nanophotonics has opened new realm of science and technology, providing breakthrough in many different fields including data processing, optical communications and holography. As one critical step in controlling light wave, nanofocusing of light is fundamental and essential in a broad range of applications such as nanolithography, surface-enhanced Raman spectroscopy (SERS), enhancement of nonlinear effects and single molecule detection. However, the diffraction limit in classical optics makes it very challenging to confine light into a deep sub-wavelength dimension. To overcome such fundamental limit, there have been active researches on nanoscale focusing, most of which have been realized by utilizing tapered plasmonic waveguides^{1–5}, structural designs such as curved geometry^{6,7} and channel plasmon-polariton modes⁸. The tapered waveguide systems ensure strong field confinement and nanometer scale resolution, but they are limited by the spatial dispersion and fabrication difficulty. Meanwhile, nanofocusing based on structural design relies on geometrical shaping of the surface in micro or nanoscale and hence it is very challenging for implementation. In this paper, we present a different approach where photons are guided by extreme anisotropy of the medium, not by physical barrier as in tapered waveguide approaches. Our system is based on hyperbolic metamaterials to achieve nanofocusing which enables confining light into a deep sub-wavelength scale as well as super-resolution imaging with an ordinary light source at the UV and visible wavelengths, which are important range in nanolithography and imaging applications.

Metamaterials, artificial materials composed of the building blocks of deep sub-wavelength size and spacing, have been an intensive research subject. Metamaterials have shown various novel properties and applications such as negative refractive index⁹, cloaking^{10,11}, sensing¹², and imaging^{13–15} since Veselago first proposed the concept in 1968¹⁶. Hyperbolic metamaterials, one intriguing and special kind of metamaterials, are a highly anisotropic material with different signs of permittivity along different axes^{17,18}. Originated from the extreme anisotropy, hyperbolic metamaterials have shown exotic properties with various applications, including all-angle negative refraction^{19–21}, sub-diffraction-limited imaging^{13,15,22}, enhancement of spontaneous emission^{23–25}, photonic spin

¹Department of Mechanical Engineering, Pohang University of Science and Technology (POSTECH), Pohang 37673, Republic of Korea. ²Department of Electrical and Computer Engineering, Northeastern University, Boston, MA 02115, USA. ³Department of Mechanical and Industrial Engineering, Northeastern University, Boston, MA 02115, USA. ⁴Department of Chemical Engineering, Pohang University of Science and Technology (POSTECH), Pohang 37673, Republic of Korea. Correspondence and requests for materials should be addressed to J.R. (email: jsrho@postech.ac.kr)

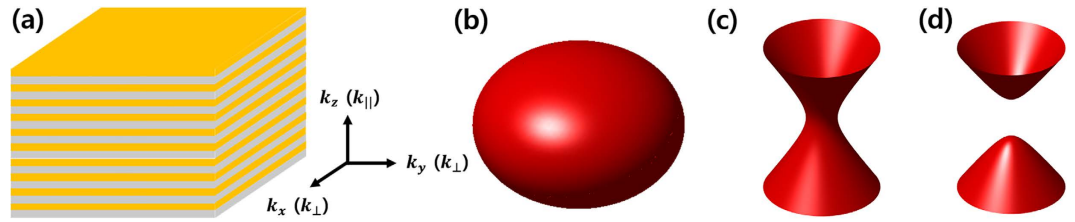


Figure 1. (a) Schematic of metal-dielectric multilayer stack. Isofrequency surface of TM waves with (b) both ε_{\perp} and ε_{\parallel} positive but not identical, (c) ε_{\perp} negative and ε_{\parallel} positive, and (d) ε_{\perp} positive and ε_{\parallel} negative. The surface normal of multilayer is defined as z-direction.

Hall effect^{26,27} and sub-wavelength waveguiding^{28,29}. To realize hyperbolic metamaterials, we can use metallic nanowires embedded in a dielectric matrix or metal-dielectric multilayer. In this paper, we will focus on the latter case. As schematically illustrated in Fig. 1(a), the hyperbolic metamaterial consists of alternating layers of metal and dielectric with thickness much smaller than the wavelength, and hence the medium can be approximated as a homogeneous medium with effective optical parameters. When wave propagates parallel to the anisotropy axis, the effective permittivity satisfies the relation as follows,

$$\varepsilon_{\perp} = \frac{\varepsilon_m d_m + \varepsilon_d d_d}{d_m + d_d}, \frac{1}{\varepsilon_{\parallel}} = \frac{d_m/\varepsilon_m + d_d/\varepsilon_d}{d_m + d_d} \quad (1)$$

where d denotes thickness of each layer, the subscripts \perp and \parallel describe components perpendicular and parallel to the propagation directions, and the subscripts m and d indicate metal and dielectric, respectively. By adapting proper geometric parameters and materials, highly anisotropic permittivity can be achieved.

For transverse magnetic (TM) waves propagating in the multilayer metamaterials, the dispersion relation is given by

$$\frac{k_{\perp}^2}{\varepsilon_{\parallel}} + \frac{k_{\parallel}^2}{\varepsilon_{\perp}} = \left(\frac{\omega}{c}\right)^2 \quad (2)$$

Here, the subscripts \perp and \parallel follow the same notation defined earlier. k is the wavevector, ε is the relative permittivity, ω is the angular frequency, and c is the speed of light in vacuum. At the frequency where the multilayer metamaterial has different signs of permittivity, the isofrequency surface exhibits hyperboloid shape as shown in Fig. 1(c) and (d), while naturally available anisotropic materials generally show ellipsoidal isofrequency surface (Fig. 1(b)).

Results

Thanks to this extraordinary dispersion relation, hyperbolic metamaterials support TM waves with transverse wave vector k_{\perp} larger than k_0 (wave vector in vacuum). Such waves are evanescent waves that cannot propagate in air, but they can be converted into propagating waves through a mechanism of angular momentum conservation in hyperlens^{30,31}. Using these properties, super-resolution imaging has been achieved by using hyperlens, a cylindrical^{13,15,22} or a spherical³² multilayer hyperbolic metamaterials from many groups.

Since the effective permittivity depends on the optical properties of the metal and dielectrics components and their filling ratio as described in equation (1), different material compositions yield different working frequency ranges. One example is shown in Fig. 2 for silver and silicon. Metal and dielectrics are properly determined to provide hyperbolic dispersion as flat as possible and high transmission for nanofocusing and super-resolution applications. For flat dispersion, real part of effective permittivity should be highly negative in radial direction and slightly positive in tangential direction, as implied in equation (2). The effective permittivity should also have small imaginary part in both radial and tangential directions in order to allow high transmission. Although realizing hyperbolic dispersion using semiconductors instead of novel metals has been reported in infrared wavelength range^{19,33}, material combinations conventionally used in visible frequency are limited to noble metals such as silver and gold and high index dielectrics because noble metals exhibit low losses whereas other metals such as aluminum are not used due to the relatively high losses.

Figure 3(a) shows a schematic design where media marked by A, B and C are air, hyperlens and silicon dioxide, respectively. The hyperlens is composed of alternatively stacked metal and dielectric in which the thickness of the each layer is set to 15 nm and outer and inner radius is 750 nm and 60 nm, respectively. If the hyperlens has ultraflat iso-frequency curve for TM waves as shown in Fig. 3(b), it can support broad range of transverse component of the wave vector and compress or expand transverse wave vector without diffraction as beam passes the hyperlens depending on its propagation direction. As waves propagate along the radial direction from inner medium (A) to outer medium (C) (yellow arrow in Fig. 3(a)), the transverse wave vector decreases from the red arrow to the orange arrow in Fig. 3(b). Therefore, evanescent waves become propagating without diffraction or distortion of the original beam shape since the direction of the group velocities which are represented by the black arrows in Fig. 3(b) barely change. Moreover, because the group velocities in the hyperlens have nearly zero transverse components, the waves propagate along the radial direction, resulting magnification of the beam size. In

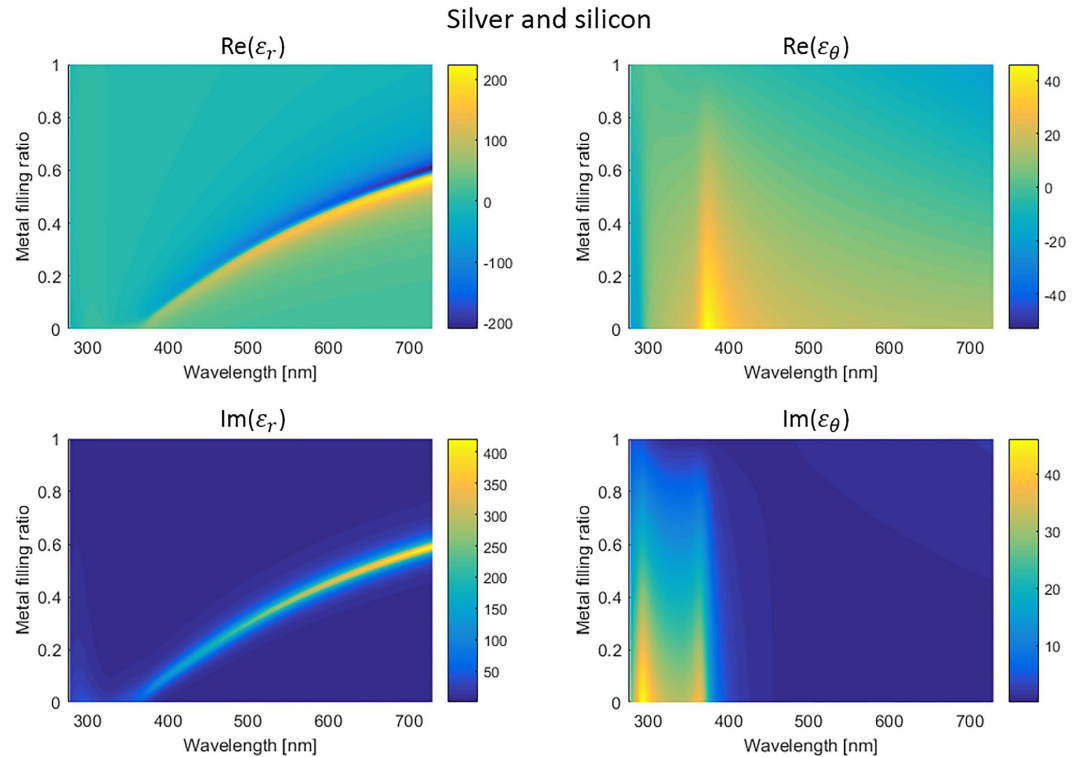


Figure 2. Effective permittivity of multilayer composed of silver and silicon.

other words, the role of the hyperlens is to convert evanescent waves into propagating waves and to magnify the image. However, if light passes the hyperlens inversely (purple arrow in Fig. 3(a)), radial propagation direction leads to compression of the incoming waves, and the incident beam will be focused into an area below the diffraction limit^{34,35}. Moreover, since the propagation of light depends on radial group velocity, highly anisotropic elliptical dispersion also supports nanofocusing with super-resolution.

Figure 3(c) and (d) are 2D simulation results of hyperlens-based nanofocusing using Finite Element Analysis since it has rotational symmetry. The incident beam is a TM-polarized Gaussian beam with beam radius of 900 nm in (c) and 400 nm in (d) both of which are easily achievable using conventional optical systems. While the incident beam exhibits a full width at half maximum (FWHM) of 817 nm in free space, the beam in the hyperlens is compressed as it propagates, resulting in 34 nm FWHM which corresponds to 0.04 of that without hyperlens. Although the intensity, which corresponds to efficiency, is reduced to half, it is still relatively high compared to imaging application due to the localization of field.

This sub-wavelength focusing can be used in applications such as nanopatterning by adding a layer with slit to the inner surface (Fig. 4(a)). Light has been an attractive source of lithography for its easy accessibility and low cost, but diffraction is a natural and fundamental phenomenon obstructing nanoscale lithography. Utilizing hyperlens, which can confine light in sub-wavelength area, a new concept of nanoscale lithography under simple UV and visible light illumination beyond the current photolithography is achievable. Intensity along the line spaced 20 nm from the layer which is marked as red dotted line is shown in Fig. 4(b). Although intensity decreases rapidly as it goes away from the focal point since it is evanescent, it is still enough for lithography application. Therefore, hyperlens is a very promising candidate for deep sub-wavelength patterning of few nanometers scale without complicated optics systems, and it can be also integrated with more complex lithography system such as flying head lithography utilizing highly focused near-field focused light³⁶.

Furthermore, this diffraction-unlimited focusing can be achieved in broad range of visible frequency by changing the materials. Figure 5 shows possible material combinations in the UV and visible range and its full-wave simulation where color map shows magnitude of Poynting vector. Here, metal filling ratio is fixed to 1/2 in all simulations. The wavelength, materials and their permittivities used in each simulation are specified under the simulation result. (The material properties are taken from literature³⁷ for gold and experimentally measured value for the remaining.) Working frequency range can be, however, further expanded by diversifying the material combinations which has not been used widely such as conventional semiconductors. Also, hyperlens can have additional degrees of freedom by adapting graphene or phase change materials (PCM). High optical tunability of graphene-based hyperlens has been recently demonstrated in the mid-infrared region by controlling the applied voltage^{38,39}, and PCM also proved characteristic optical properties which is tunable in the vicinity of the phase transition by tuning temperature in near-infrared regime^{40,41}. If one can apply these schemes in the visible range, single material combination can cover whole range of optical frequencies by simply tuning voltage or temperature, opening new possibilities in both nanofocusing and imaging area.

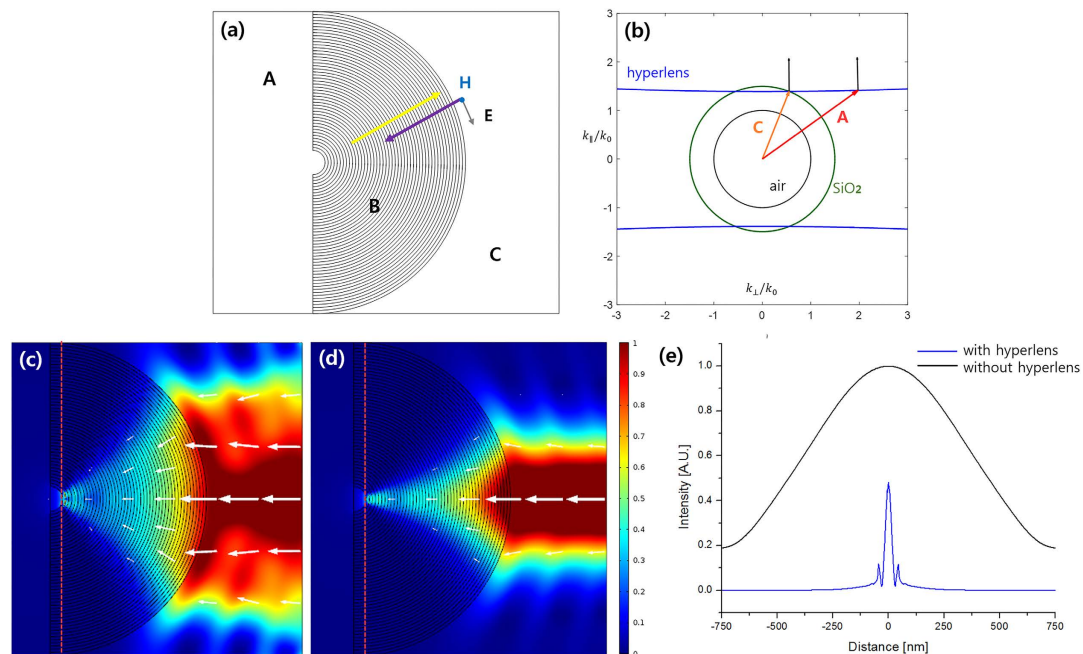


Figure 3. Schematic and 2D simulation of the hyperlens-based nanofocusing. (a) Schematic design. Media denoted by A, B and C are air, hyperlens and silicon dioxide, respectively. Yellow and purple arrows denote Poynting vector of outgoing and incoming TM waves, respectively. (b) Two-dimensional isofrequency curve for TM waves in hyperlens consisting of silver and silicon (blue), compared to the isofrequency curve of silicon dioxide (green) and air (black) at wavelength 560 nm. Red and orange arrows marked by A and C indicate wave vectors supported by the media of A and C in (a), and the black arrows indicate the direction of group velocities in the hyperlens. (c) and (d) Intensity profile in the hyperlens composed of silver and silicon with incident beam radius of (c) 900 nm and (d) 400 nm and white arrows denote Poynting vector. (e) Normalized intensity along red dotted line when the incident beam has radius of 400 nm.

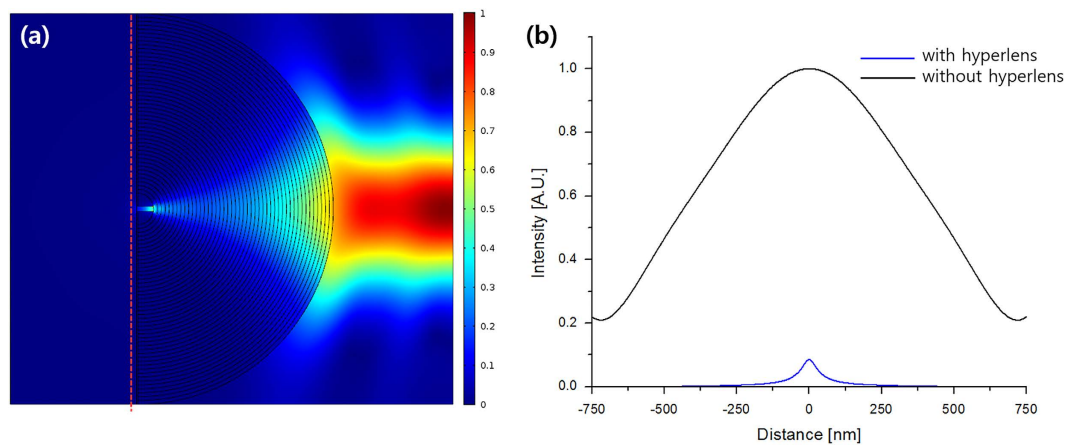


Figure 4. Hyperlens-based nanofocusing where chrome layer with slit is added to the inner surface. (a) Intensity profile in the hyperlens consisting of silver and silicon at wavelength of 560 nm. (b) Normalized intensity along the vertical line spaced 20 nm from the chrome layer which is indicated as red dotted line. The width of the slit is set to 20 nm.

In conclusion, hyperlens-based nanofocusing system provides both deep sub-wavelength confinement of light and super-resolution imaging by controlling the spot size in nanometer scale without complex optics system such as electron beam lithography, ion beam lithography and deep-UV photolithography. We have numerically showed light localization originated from nearly-flat hyperbolic dispersion and suggested various material combinations to cover parts of UV and whole visible range. Introducing tunable materials such as graphene and PCM will bring useful applications which remains as future works. Although fabrication of the hyperlens system is challenging

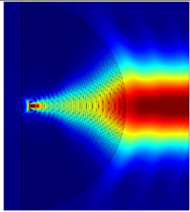
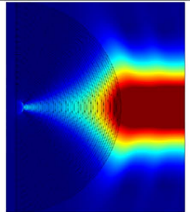
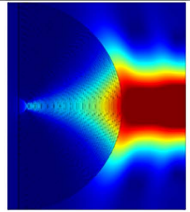
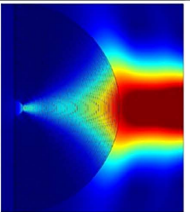
Wavelength [nm]	300-400	400-500	500-600	600-700
Metal	Silver	Silver	Silver	Gold
Dielectric	SiO ₂ , Al ₂ O ₃ , ITO, Si ₃ N ₄	TiO ₂	Silicon, GaAs	Silicon, GaAs
Full-wave Simulation Results	 At 365 nm Ag (-2.5753+0.2453i) Al ₂ O ₃ (3.2161)	 At 410 nm Ag (-4.9816+0.2233i) TiO ₂ (5.83)	 At 560 nm Ag (-13.5289+0.4164i) Si (17.3830+0.8560i)	 At 640 nm Au (-11.036+1.2619i) Si (14.974 +0.14163i)

Figure 5. Materials according to the operating wavelength spanning 300 nm to 700 nm where metal filling ratio is 1/2. Color maps indicate the magnitude of Poynting vector. Wavelength and materials (permittivity) used for the simulation are shown.

because of their requirement of geometry definition and multi-level thin-film deposition process, it could be further improved with the on-going researches in scalable nanofabrication processes such as roll-to-roll system and pattern transfer techniques. Further, the proposed deep sub-wavelength nanofocusing property of hyperlens can be applied to not only low-cost and high-resolution nanoscale lithography, but also several other interesting applications such as SERS and single molecule level imaging with the extremely focused near-field light.

Methods

We used COMSOL Multiphysics 5.0 for numerical simulation.

References

- Stockman, M. I. Nanofocusing of Optical Energy in Tapered Plasmonic Waveguides. *Phys. Rev. Lett.* **93**, 137404 (2004).
- Davoyan, A. R., Shadrivov, I. V., Zharov, A. A., Gramotnev, D. K. & Kivshar, Y. S. Nonlinear Nanofocusing in Tapered Plasmonic Waveguides. *Phys. Rev. Lett.* **105**, 116804 (2010).
- Verhagen, E., Polman, A. & Kuipers, L. Nanofocusing in laterally tapered plasmonic waveguides. *Opt. Express* **16**, 45–57 (2008).
- Choo, H. *et al.* Nanofocusing in a metal-insulator-metal gap plasmon waveguide with a three-dimensional linear taper. *Nature Photon.* **6**, 838–844 (2012).
- Lindquist, N. C., Nagpal, P., Lesuffleur, A., Norris, D. J. & Oh, S.-H. Three-Dimensional Plasmonic Nanofocusing. *Nano Lett.* **10**, 1369–1373 (2010).
- Ma, C. & Liu, Z. Focusing light into deep subwavelength using metamaterial immersion lenses. *Opt. Express* **18**, 4838–4844 (2010).
- Shi, H., Du, C. & Luo, X. Focal length modulation based on a metallic slit surrounded with grooves in curved depths. *Appl. Phys. Lett.* **91**, 093111 (2007).
- Volkov, V. S. *et al.* Nanofocusing with Channel Plasmon Polaritons. *Nano Lett.* **9**, 1278–1282 (2009).
- Shelby, R. A., Smith, D. R. & Schultz, S. Experimental Verification of a Negative Index of Refraction. *Science* **292**, 77–79 (2001).
- Leonhardt, U. Optical conformal mapping. *Science* **312**, 1777–1780 (2006).
- Pendry, J. B., Schurig, D. & Smith, D. R. Controlling electromagnetic fields. *Science* **312**, 1780–1782 (2006).
- Kabashin, A. *et al.* Plasmonic nanorod metamaterials for biosensing. *Nature Mater.* **8**, 867–871 (2009).
- Jacob, Z., Alekseyev, L. V. & Narimanov, E. Optical Hyperlens: Far-field imaging beyond the diffraction limit. *Opt. Express* **14**, 8247–8256 (2006).
- Pendry, J. B. Negative Refraction Makes a Perfect Lens. *Phys. Rev. Lett.* **85**, 3966–3969 (2000).
- Salandrino, A. & Engheta, N. Far-field subdiffraction optical microscopy using metamaterial crystals: Theory and simulations. *Phys. Rev. B* **74**, 075103 (2006).
- Veselago, V. G. The electrodynamics of substances with simultaneously negative values of ϵ and μ . *Sov. Phys. Usp.* **10**, 509–514 (1968).
- Ferrari, L., Wu, C., Lepage, D., Zhang, X. & Liu, Z. Hyperbolic metamaterials and their applications. *Prog. in Quant. Electron.* **40**, 1–40 (2015).
- Guo, Y., Newman, W., Cortes, C. L. & Jacob, Z. Applications of Hyperbolic Metamaterial Substrates. *Adv. in OptoElectron.* **2012**, 9 (2012).
- Hoffman, A. J. *et al.* Negative refraction in semiconductor metamaterials. *Nature Mater.* **6**, 946–950 (2007).
- Liu, Y., Bartal, G. & Zhang, X. All-angle negative refraction and imaging in a bulk medium made of metallic nanowires in the visible region. *Opt. Express* **16**, 15439–15448 (2008).
- Yao, J. *et al.* Optical Negative Refraction in Bulk Metamaterials of Nanowires. *Science* **321**, 930–930 (2008).

22. Liu, Z., Lee, H., Xiong, Y., Sun, C. & Zhang, X. Far-Field Optical Hyperlens Magnifying Sub-Diffraction-Limited Objects. *Science* **315**, 1686–1686 (2007).
23. Lu, D., Kan, J. J., Fullerton, E. E. & Liu, Z. Enhancing spontaneous emission rates of molecules using nanopatterned multilayer hyperbolic metamaterials. *Nature Nanotechnol.* **9**, 48–53 (2014).
24. Slobozhanyuk, A. P. *et al.* Purcell effect in hyperbolic metamaterial resonators. *Phys. Rev. B* **92**, 195127 (2015).
25. Ferrari, L., Lu, D., Lepage, D. & Liu, Z. Enhanced spontaneous emission inside hyperbolic metamaterials. *Opt. Express* **22**, 4301–4306 (2014).
26. Kapitanova, P. V. *et al.* Photonic spin Hall effect in hyperbolic metamaterials for polarization-controlled routing of subwavelength modes. *Nature Commun.* **5** (2014).
27. High, A. A. *et al.* Visible-frequency hyperbolic metasurface. *Nature* **522**, 192–196 (2015).
28. Ishii, S., Shalaginov, M. Y., Babicheva, V. E., Boltasseva, A. & Kildishev, A. V. Plasmonic waveguides clad by hyperbolic metamaterials. *Opt. Lett.* **39**, 4663–4666 (2014).
29. He, Y., He, S. & Yang, X. Optical field enhancement in nanoscale slot waveguides of hyperbolic metamaterials. *Opt. Lett.* **37**, 2907–2909 (2012).
30. Podolskiy, V. A. & Narimanov, E. E. Strongly anisotropic waveguide as a nonmagnetic left-handed system. *Phys. Rev. B* **71**, 201101 (2005).
31. Govyadinov, A. A. & Podolskiy, V. A. Meta-material photonic funnels for sub-diffraction light compression and propagation. *Phys. Rev. B* **73**, 155108 (2006).
32. Rho, J. *et al.* Spherical hyperlens for two-dimensional sub-diffractive imaging at visible frequencies. *Nature Commun.* **1**, 143 (2010).
33. Naik, G. V., Liu, J., Kildishev, A. V., Shalae, V. M. & Boltasseva, A. Demonstration of Al:ZnO as a plasmonic component for near-infrared metamaterials. *Proc. Natl. Acad. Sci. USA* **109**, 8834–8838 (2012).
34. Xiong, Y., Liu, Z. & Zhang, X. A simple design of flat hyperlens for lithography and imaging with half-pitch resolution down to 20 nm. *Appl. Phys. Lett.* **94**, 203108 (2009).
35. Wan, W., Ponsetto, J. L. & Liu, Z. Numerical study of hyperlenses for three-dimensional imaging and lithography. *Opt. Express* **23**, 18501–18510 (2015).
36. Pan, L. *et al.* Maskless Plasmonic Lithography at 22|nm Resolution. *Sci. Rep.* **1**, 175 (2011).
37. Rakić, A. D., Djurišić, A. B., Elazar, J. M. & Majewski, M. L. Optical properties of metallic films for vertical-cavity optoelectronic devices. *Appl. Opt.* **37**, 5271–5283 (1998).
38. Li, P. & Taubner, T. Broadband subwavelength imaging using a tunable graphene lens. *ACS Nano* **6**, 10107–10114 (2012).
39. Zhang, T., Chen, L. & Li, X. Graphene-based tunable broadband hyperlens for far-field subdiffraction imaging at mid-infrared frequencies. *Opt. Express* **21**, 20888–20889 (2013).
40. Qazilbash, M. M. *et al.* Mott Transition in VO₂ Revealed by Infrared Spectroscopy and Nano-Imaging. *Science* **318**, 1750–1753 (2007).
41. Shportko, K. *et al.* Resonant bonding in crystalline phase-change materials. *Nature Mater.* **7**, 653–658 (2008).

Acknowledgements

The research was supported by Young Investigator Research program (NRF-2015R1C1A1A02036464), Engineering Research Center program (NRF-2015R1A5A1037668) and Global Frontier program (CAMM-2014M3A6B3063708) through the National Research Foundation of Korea (NRF) grant funded by the Ministry of Science, ICT and Future Planning (MSIP) of Korean government.

Author Contributions

J.R. conceived the idea and guided the research. M.K. did numerical simulations. S.S., K.Y. and Y.L. suggested the idea of materials characterizations. M.K., S.S., K.Y., Y.L. and J.R. wrote the manuscript. All authors participated in the discussion and approved the final manuscript.

Additional Information

Competing financial interests: The authors declare no competing financial interests.

How to cite this article: Kim, M. *et al.* Deep sub-wavelength nanofocusing of UV-visible light by hyperbolic metamaterials. *Sci. Rep.* **6**, 38645; doi: 10.1038/srep38645 (2016).

Publisher's note: Springer Nature remains neutral with regard to jurisdictional claims in published maps and institutional affiliations.



This work is licensed under a Creative Commons Attribution 4.0 International License. The images or other third party material in this article are included in the article's Creative Commons license, unless indicated otherwise in the credit line; if the material is not included under the Creative Commons license, users will need to obtain permission from the license holder to reproduce the material. To view a copy of this license, visit <http://creativecommons.org/licenses/by/4.0/>

© The Author(s) 2016